Ionics (2014) 20:1737–1745
DOI 10.1007/s11581-014-1073-8

ORIGINAL PAPER

Effect of molybdenum doping on the electrochromic properties of tungsten oxide thin films by RF magnetron sputtering

V. Madhavi · P. Jeevan Kumar · P. Kondaiah · O. M. Hussain · S. Uthanna

Received: 22 October 2013 / Revised: 20 December 2013 / Accepted: 11 January 2014 / Published online: 27 April 2014

Abstract Thin films of pure and molybdenum (Mo)-doped tungsten trioxide (WO_3) were deposited on indium tin oxide (ITO)-coated glass and Corning glass substrates by RF magnetron sputtering technique. The effect of Mo doping on the structural, morphological, optical and electrochromic properties of WO_3 films was studied systematically. The energy dispersive X-ray analysis (EDAX) revealed that the films consist of molybdenum concentrations from 0 to 2 at.%. X-ray diffraction (XRD) studies indicated that with the increase of Mo concentration the structural phase transformation takes place from polycrystalline to amorphous phase. The crystallite size of the films decreased from 24 to 12 nm with increase of doping concentration of Mo in WO_3. Scanning electron microscope (SEM) analysis revealed that Mo dopant led to significant changes in the surface morphology of the films. The electrochemical and electrochromic performance of the pure and Mo-doped WO_3 were studied. The WO_3 films formed with 1.3 at.% Mo dopant concentration exhibited high optical modulation of 44.3 % and coloration efficiency of 42.5 cm^2/C.

Keywords Molybdenum · Doping · Tungsten trioxide · RF magnetron sputtering

Introduction

Transition metal oxides such as tungsten trioxide, titanium dioxide, nickel oxide, iridium oxide, vanadium oxide and molybdenum oxide have shown considerable application in the areas of electrochromic, gas sensors and lithium ion batteries [1–6]. Zheng et al. [7] synthesized nanostructured WO_3 films using different methods for traditional applications like electrochromic, gas sensors and photocatalysis. In addition, these films are also used in dye-sensitized solar cells, optical data storage, field-emission displays and high-T_c superconductors. Among these, tungsten trioxide (WO_3) has been exhibited good electrochromic properties. The electrochromic effect observed in these materials has led to their use in the development of display devices and smart windows. The development of new and improved electrochromic devices depends on enhancement in the color efficiency. However, the color efficiency of the electrochromic device can also be modified by doping suitable metal ions with lower oxidizing capacity than the host materials. Faughnan and Crandall [8] reported that the higher electrochromic efficiencies are expected as a result of enhanced electron intervalence transfer between Mo^{5+} and W^{6+} states, in addition Mo^{5+} to Mo^{6+} and W^{5+} to W^{6+} transitions. The high color efficiency depends on the rate of intercalation that is coloration under applied electric field and controlled by the charge transfer at the WO_3/electrolyte interface, which critically depend on the surface texture, defect structure and dopant content of the films. There are several reports on the titanium [8], niobium and vanadium [9] and nickel [10] doped WO_3 films deposited by different techniques. Penin et al. [11] prepared $Mo_xW_{1-x}O_3$ (x=0–1) films by cathodic electrodeposition technique, and they reported the structure, composition and electrochemical associated lithium-insertion properties of mixed molybdenum and tungsten oxide films. Kondrachova et al. [12] have reported that the mixed MoO_3-WO_3 films exhibited better electrochromic properties compared to binary oxide films. Gesheva et al. [13] deposited Mo-doped (0–10 at.%) WO_3 films by spray

V. Madhavi (✉) · P. Kondaiah · O. M. Hussain · S. Uthanna
Department of Physics, Sri Venkateswara University,
Tirupati 517502, India
e-mail: madhuvphysics@gmail.com

P. J. Kumar
Department of Physics, Nitte Meenakshi Institute of Technology
(NMIT), Bangalore 560069, India

pyrolysis and studied their electrochromic response. Rueda de Leon et al. [14] and Kalidindi et al. [15, 16] studied the effect of substrate temperature on crystallite structure, phase and electrical conductivity of Ti-doped WO_3 films deposited RF magnetron sputtering technique. In this investigation, we report the influence of Mo dopant concentration in WO_3 films prepared by RF magnetron sputtering technique on the structural and morphological, optical and electrochromic properties.

Experimental

Pure and Mo-doped WO_3 thin films were deposited on glass and ITO-coated glass substrates by RF magnetron sputtering technique. The vacuum pumping system was employed for sputter deposition uses a combination of diffusion and rotary pumps to achieve an ultimate pressure of 4×10^{-4} Pa. Pure oxygen and argon were used as reactive and sputter gases, respectively. Required quantities of oxygen and argon gases were admitted into the sputter chamber through fine controlled needle valves and their flow rates were monitored individually employing Aalborg mass flow controllers. Digital Pirani and Penning gauges were used to measure the pressure in the sputter chamber. The target to substrate distance was kept at 5 cm. The films were deposited at a fixed substrate temperature of 473 K, oxygen partial pressure of 6×10^{-2} Pa and sputter pressure of 4 Pa. The RF power applied to the sputter target was 150 W, and the deposition time was 120 min. Molybdenum doping was achieved by selectively masking of an erosion portion of the tungsten target by pure molybdenum strips of different sizes. The chemical composition of the films estimated by using energy dispersive X-ray analyser (Philips XL 308) attached to scanning electron microscope. Structural properties was investigated by X-ray diffraction (XRD) technique (Siefent model 3003TT) with Cu Kα radiation source (λ= 0.15406 nm). Surface morphology was studied by scanning electron microscopy (Hitachi SEM model S-400). The optical transmittance of the films was recorded by UV–Vis–NIR spectrophotometer (Perkin Elmer model Lambda 950) in the wavelength range 300–1500 nm.

The electrochromic and electrochemical properties of the pure and Mo-doped WO_3 films were studied by three-electrode cell configuration with platinum as a counter electrode and calomel electrode as a reference electrode and pure and doped WO_3 films formed on ITO-coated glass as a working electrode. The cyclic voltammetry experiments were performed by varying the potential in the range from +1 to −1 V in the electrolyte solution of 1 M Li_2SO_4 and at a scan rate of 50 mV/s. The colored and bleached states of the films were recorded using the spectrophotometer.

Results and discussions

Chemical composition

The chemical composition of the pure and Mo-doped WO_3 films deposited on glass substrates were determined by using EDAX analysis. Figure 1 shows the EDAX spectra of pure and Mo-doped WO_3 films formed with different concentrations. Figure 1a shows the characteristics peaks of tungsten and oxygen. The chemical component present in the films calculated from the intensity of the peaks was 25.9 at.% of tungsten and 74.1 at.% of oxygen and with the ratio of oxygen to tungsten found to be 2.96, which indicated the grown the WO_3 films of nearly stoichiometric. Figure 1b, c and d clearly shows that the additional peaks were related to the molybdenum along with tungsten and oxygen. It was found that the intensity of molybdenum peak increased with the increase in the area of the molybdenum strips fixed on the sputter target of tungsten. The atomic percent of oxygen, tungsten and molybdenum present in the films are listed in Table 1. The estimated molybdenum atomic percentages present in the WO_3 films were found to be 0.9, 1.3 and 2.0 at.%.

Structural properties

Figure 2 shows the XRD patterns of pure and Mo-doped WO_3 films deposited on ITO-coated glasses substrates formed at the substrate temperature of 473 K. From the XRD patterns, it was observed that the pure WO_3 films showed a weak diffraction peak at 2θ=23.5° related to the (020) reflection of orthorhombic phase of WO_3 (JCPDS Card No. 89-4480) in the amorphous matrix. For the films formed with 0.9 at.% of Mo doping, the intensity of the (020) reflection peak was increased and a new weak diffraction peak seen at 2θ=22.8° which related to the (002) reflection of WO_3. For films doped with Mo 1.3 at.%, the intensity of the (002) peak was increased where as the intensity of (020) reflection was found to decreased. The presence of two additional peaks observed at 26.7° and 35.2° related to the (120) and (122) reflections of WO_3 which indicated that the grown films were of polycrystalline in nature. Such orthorhombic WO_3 phase was also achieved in titanium-doped (1–10 wt.%) WO_3 films deposited by pulsed laser deposition technique [17] and nitrogen-doped WO_3 films formed by pulsed laser deposition [18]. At further increase of Mo dopant content to 2 at.%, the films exhibited an amorphous nature. In all films, there was no diffraction peaks related to either metallic molybdenum or MoO_3, which clearly indicated that the molybdenum substituted in the tungsten sites in WO_3 due to the same size of their ionic radii (73 pm for Mo^{+6} and 74 pm for W^{+6}). Bathe and Patil [9] also reported the polycrystalline to amorphous phase transformation with increase of titanium doping from 2 at.% to 6 at.% in WO_3 films formed by pulsed spray pyrolysis

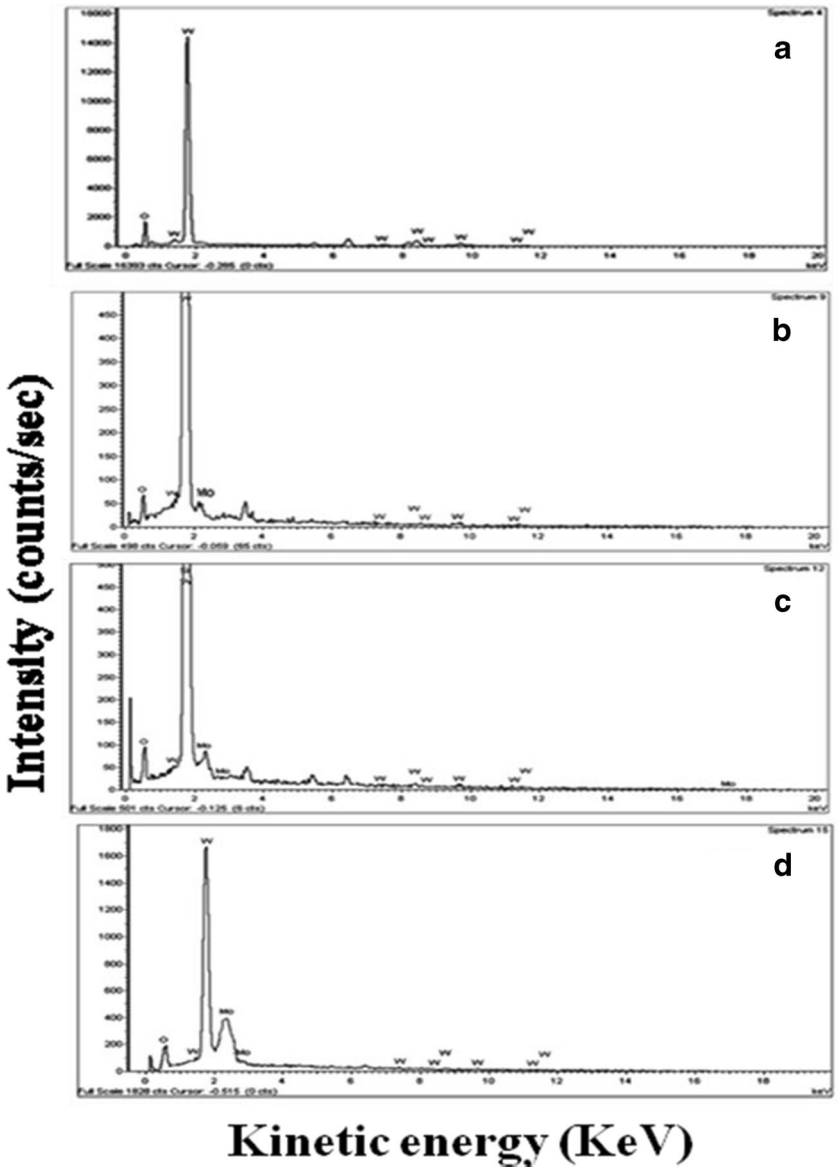

Fig. 1 EDAX spectra of **a** pure WO_3, **b** 0.9 at.%, **c** 1.3 at.% and **d** 2.0 at.% Mo-doped WO_3 films deposited on glass substrates formed at substrate temperature of 473 K

technique. The crystallite size (L) of the films was calculated by using Debye–Scherrer's relation [19],

$$L = 0.9\lambda/\beta\cos\theta, \quad (1)$$

where λ is the wavelength of the X-rays, β is the full width at half-maximum of diffraction intensity in radians and θ is the diffraction angle. The crystallite size of the films formed with 0.9 at.% of Mo was 24 nm, and it decreased to 12 nm for the films doped with 1.3 at.% of Mo. The incorporated molybdenum inhibits the grain growth in WO_3 matrix. Lethy et al. [17] also observed the suppression of the grain growth in titanium-doped WO_3 films by incorporation of titanium ions which interfering into the intergranules and thereby introducing sufficient pinning force. The incorporated titanium ions can inhibit the grain boundary mobility or modify the interfacial tension/surface energy leading to a decrease in grain growth velocity or nucleation energy barrier, resulting in reduction in grain size. The similar nature of decrement in the crystallite size was observed in lithium-doped WO_3 films [20].

Table 1 Elemental composition of pure Mo-doped WO_3 films deposited on glass substrates determined by EDAX

Films	Oxygen (at.%)	Tungsten (at.%)	Molybdenum (at.%)
(a)	74.1	25.9	0
(b)	72.9	26.2	0.9±0.02
(c)	73.3	25.4	1.3±0.02
(d)	74.1	23.9	2.0±0.02

It is to be noted that the value of 2θ shifted to higher angle side with the increase of Mo doping which modifies the lattice

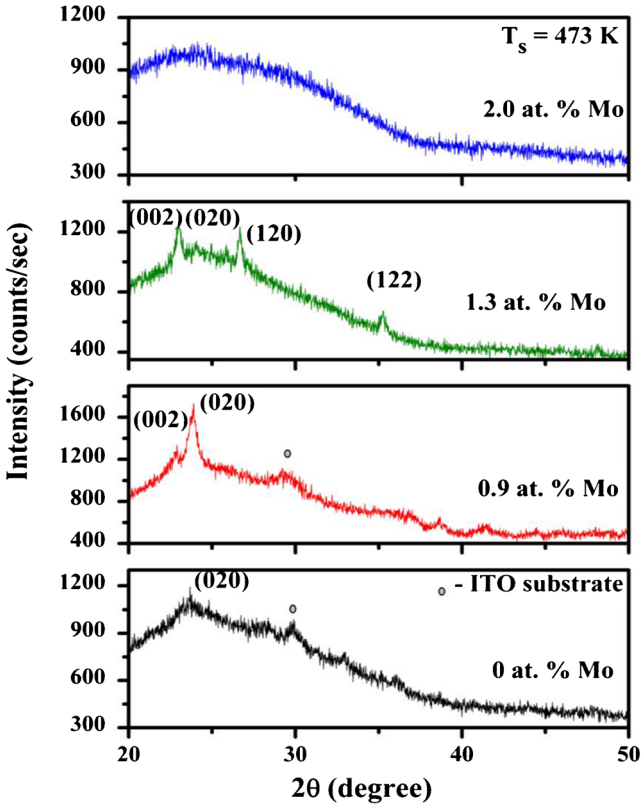

Fig. 2 XRD profiles of pure and Mo-doped WO_3 films deposited on ITO-coated glass substrates formed at substrate temperature of 473 K

parameters. The lattice constants *a*, *b*, and *c* of the films are calculated using the formula

$$1/d^2 = h^2/a^2 + k^2/b^2 + l^2/c^2, \quad (2)$$

where *d* is the interplanar distance, and *h*, *k*, *l* are Miller indices. The lattice parameters are calculated from the position of diffraction peaks are found to be *a*=7.409 Å, *b*=7.4714 Å and *c*=7.788 Å for the films doped with 1.3 at.% Mo. For WO_3 films the standard values of lattice parameters are *a*=7.3902, *b*=7.5655 and *c*=7.7875 (JCPDS Card number 89-4480). It is observed that the small change in lattice parameters can be attributed to the increase of cation size in the octahedral site with the substitution of molybdenum ions into the tungsten ion lattice.

The strain developed in the films was calculated using the relation.

$$\varepsilon = \beta \cos\theta/4, \quad (3)$$

where β is the full width at half-maximum and θ is the diffraction angle. The strain of the films increased from 1×10^{-1} to 1.6×10^{-1} with increase of Mo concentration from 0.9 to 1.3 at.%, respectively. There is not much variation in the lattice strain due to the same atomic radii of tungsten and molybdenum.

Surface morphology

The surface morphology of the pure and Mo-doped WO_3 films deposited on glass substrates were examined using SEM. Figure 3a–d shows the scanning electron microscope images of pure and Mo-doped WO_3 films. Figure 3a confirms the spherical grain growth in pure WO_3 films, and the size of the grains was around 70 nm. For Mo-doped (0.9 at.%) WO_3 films, the agglomeration of grains observed and the average grain size was 45 nm as shown in Fig. 3b. The leaf-like grain structures was observed at 1.3 at.% of Mo-doped films with grain size of 60 nm (Fig. 3c). The films formed with 2 at.% of Mo exhibited completely different morphology in which agglomerated grain structure disappeared as shown in Fig. 3d.

Optical properties

Optical transmittance spectra of pure and Mo-doped WO_3 films deposited on glass substrates in the wavelength region of 300–1500 nm are shown in Fig. 4. All the films showed high transmittance in the visible range with an average transmittance varied between 80 % and 75 %. Papadimitropoulos et al. [21] reported the high optical transmittance of 90 % for pure WO_3 films prepared by hotwire deposition technique. The absorption edge shifted towards the lower wavelength with increase of Mo dopant, indicating the increase in the optical band gap with dopant concentration of molybdenum. The optical absorption coefficient (α) of the films was calculated from the optical transmittance (*T*) data using the relation,

$$\alpha = -(1/t)\ln T, \quad (4)$$

where *t* is the film thickness. The optical absorption in the films was fitted to the Tauc's relation assuming that the direct transitions were takes place from the top of the valance band and bottom of the conduction band as given by the relation,

$$(\alpha h\upsilon)^2 = A\left(h\upsilon - E_g\right) \quad (5)$$

Figure 5 shows the plots of $(\alpha h\upsilon)^2$ versus photon energy ($h\upsilon$) of pure and Mo dopant of WO_3 films. It is observed that the optical band gap of the films was found to increased from 3.21 to 3.33 eV with the increase of dopant concentration of Mo from 0 to 2 at.%, respectively. Gullapalli et al. [22] reported the optical band gap value 3.17 eV for pure WO_3 films deposited at substrate temperature of 473 K. The increase in the optical band gap with Mo dopant concentration is due to the Moss–Burstein shift. Gaury et al. [23] also noticed such increase in the band gap in Nb-doped WO_3 films. The refractive index (*n*) of the films was determined from the optical transmittance

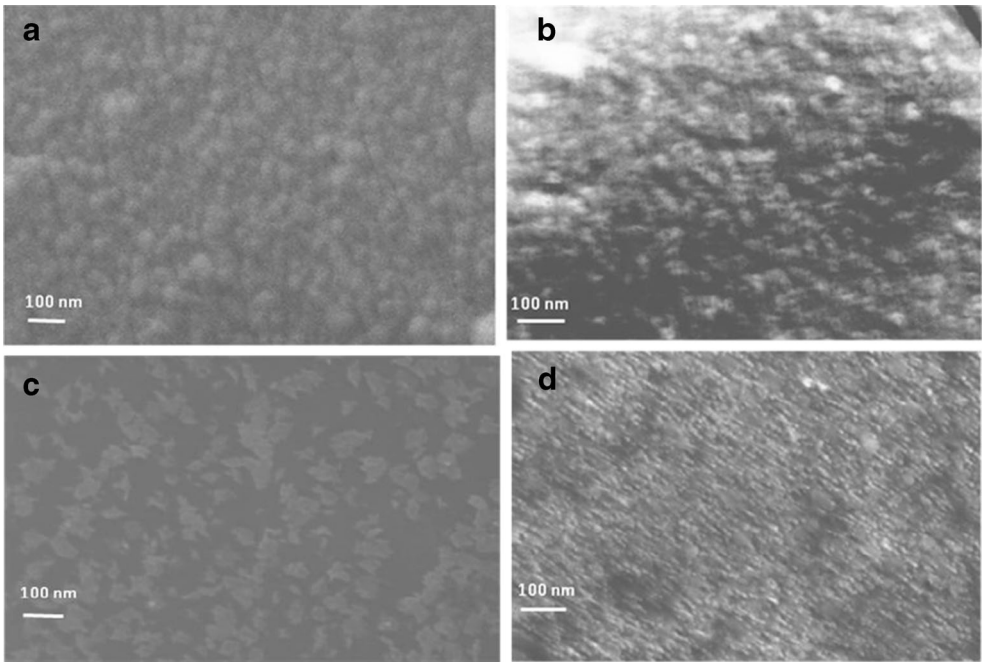

Fig. 3 SEM images of **a** pure WO_3, **b** 0.9 at.%, **c** 1.3 at.% and **d** 2.0 at.% Mo-doped WO_3 films deposited on glass substrates formed at substrate temperature of 473 K

interference data employing Swanepoel's envelope method [24] using the relation

$$n(\lambda) = \left[N + \left(N^2 - {n_0}^2 {n_1}^2\right)^{1/2}\right]^{1/2} \quad (6)$$

and

$$N = 2n_0 n_1 [(T_{max} - T_{min})/T_{max} T_{min}] + \left({n_0}^2 + {n_1}^2\right)/2, \quad (7)$$

where n_0 and n_1 are the refractive indices of air and substrate, and T_{max} and T_{min} are the successive optical transmittance maxima and minima, respectively. Figure 6 shows the wavelength dependence of refractive index of pure and Mo-doped WO_3 films. In all films, the refractive index of the films decreased with the increase of wavelength and remain almost constant at higher wave length region. At a fixed wavelength of 550 nm, the refractive index of the films increased from 2.12 to 2.25 with increase of molybdenum dopant concentration from 0 to 2 at.%, respectively.

Electrochemical properties

Figure 7 shows the cyclic voltammograms of pure and Mo-doped WO_3 films recorded at the scan rate of 50 mV/s in a 1 M Li_2SO_4 electrolyte solution. From the figure, it is observed that as the potential decreased from +1 to −1 V a progressive

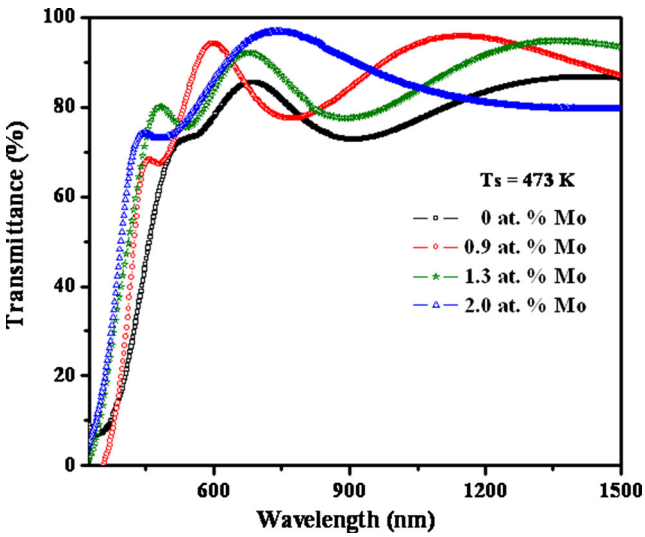

Fig. 4 Optical transmittance of pure and Mo-doped WO_3 films deposited on glass substrates formed at substrate temperature of 473 K

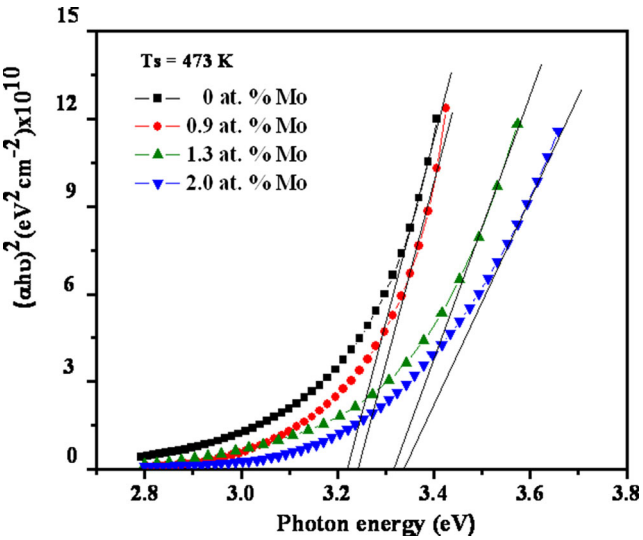

Fig. 5 Plots of $(\alpha h\nu)^2$ versus photon energy of pure and Mo-doped WO_3 films

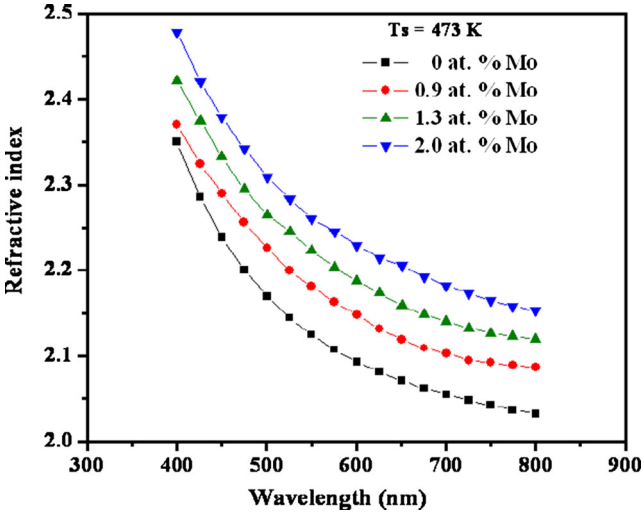

Fig. 6 Variation of refractive index with wavelength of pure and Mo-doped WO_3 films deposited on glass substrates formed at substrate temperature of 473 K

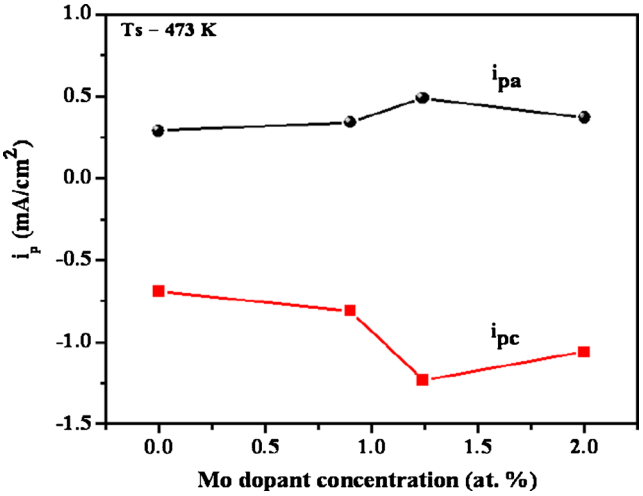

Fig. 8 Variation of anodic and cathodic peaks with Mo doping concentration in WO_3 films

increase in the cathodic current peaks associated with the reduction of $W^{6+} \rightarrow W^{5+}$ due to the Li^+ ion insertion in the films. These processes lead to the coloration in the films. Reversing the potential from −1 to +1, the anodic current peaks are observed and the colored films transformed to transparent due to the oxidation of $W^{5+} \rightarrow W^{6+}$. Figure 7 shows that anodic potential shifted towards positive potential from −0.05 to 0.15 V with increase of Mo dopant in WO_3 films. A shift in anodic peak potential indicated that the energy required for extracting the intercalated Li^+ ions from the film decreased with increase of Mo dopant in WO_3. The magnitude of CV curves was increased with the increase of Mo dopant up to 1.3 at.% due to the intercalation of a greater number of Li^+ ions in the films. The enhancement lies in the rearrangement of WO_3 structure by substitution of tungsten with molybdenum. Patil et al. [25] also noticed an increase in the area of CV plots with increase of Mo-doped V_2O_5 films due to easy way to diffusion and charge transfer process of ions. Mahajan et al. [26] also reported such an improvement in the CV performance in Ti-doped MoO_3 films may be due to the Ti^{4+} supported the Mo^{6+} to Mo^{5+} reaction. The anodic and cathodic current densities as a function of Mo dopant in WO_3 films are shown in Fig. 8. It is clearly observed that the anodic current density increased from 0.29 to 0.49 mA/cm^2 for pure to 1.3 at.% Mo-doped WO_3 films thereafter it decreased to 0.37 mA/cm^2 with further increase of Mo concentration to 2 at.% due to the fewer Li^+ ions participated in the reaction. The insertion of Li^+ ions depends on the diffusion coefficient and density of the films. The diffusion coefficient (D) of Li^+

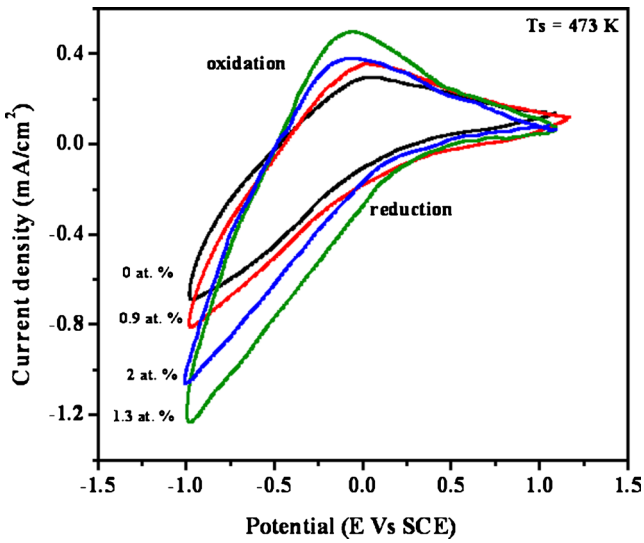

Fig. 7 Cyclic voltammetry (*CV*) of pure and Mo-doped WO_3 films formed on ITO-coated glass substrates formed at substrate temperature of 473 K

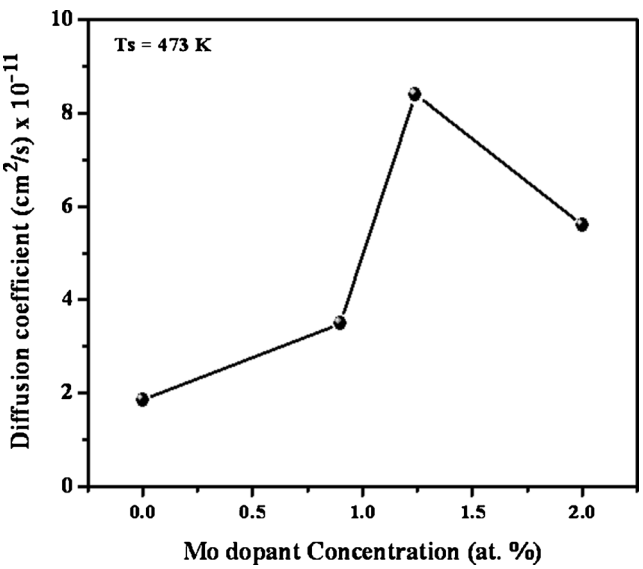

Fig. 9 Variation of diffusion coefficient with Mo dopant concentration in WO_3 films

ions during intercalation and de-intercalation process was calculated using Randles–Servik equation [27],

$$D^{1/2} = i_p / \left[\left(2.72 \times 10^5\right) n^{3/2} A C_o \nu^{1/2} \right], \quad (8)$$

where i_p is the anodic peak current density, n the number of electrons transferred in the redox reaction (which is assumed to be unity), C_o is the concentration of active ions in the solution, ν is the scan rate and A is the area of the film.

Figure 9 shows the dependence of diffusion coefficient on the content of molybdenum doping concentration in the WO_3 films. It is seen from the figure that the diffusion coefficient increased from 1.85×10^{-11} to $8.5\times10^{\times11}$ cm^2/s with the increase of Mo dopant concentration from 0 to 1.3 at.%; thereafter, it decreased to 5.6×10^{-11} cm^2/s with the further increase of Mo dopant concentration to 2.0 at.%. This could be due to the variation in the mobility of Li^+ ions in the redox reaction. Leon et al. [14] observed that the diffusion coefficient increased from 4.07×10^{-12} to 6.30×10^{-11} cm^2/s with the increase of Mo dopant concentration.

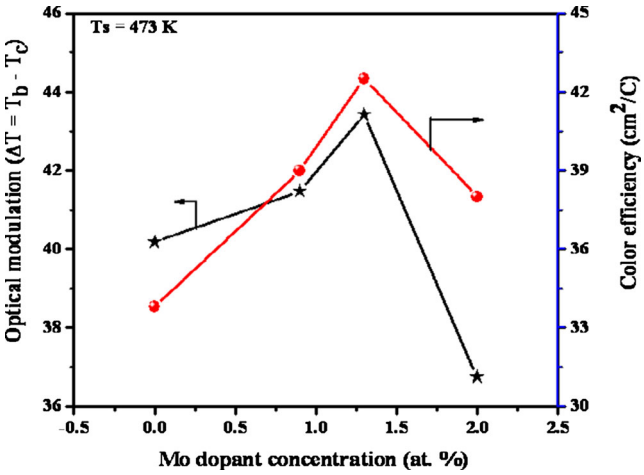

Fig. 11 Dependence of coloration efficiency on Mo doping concentration in WO_3 films

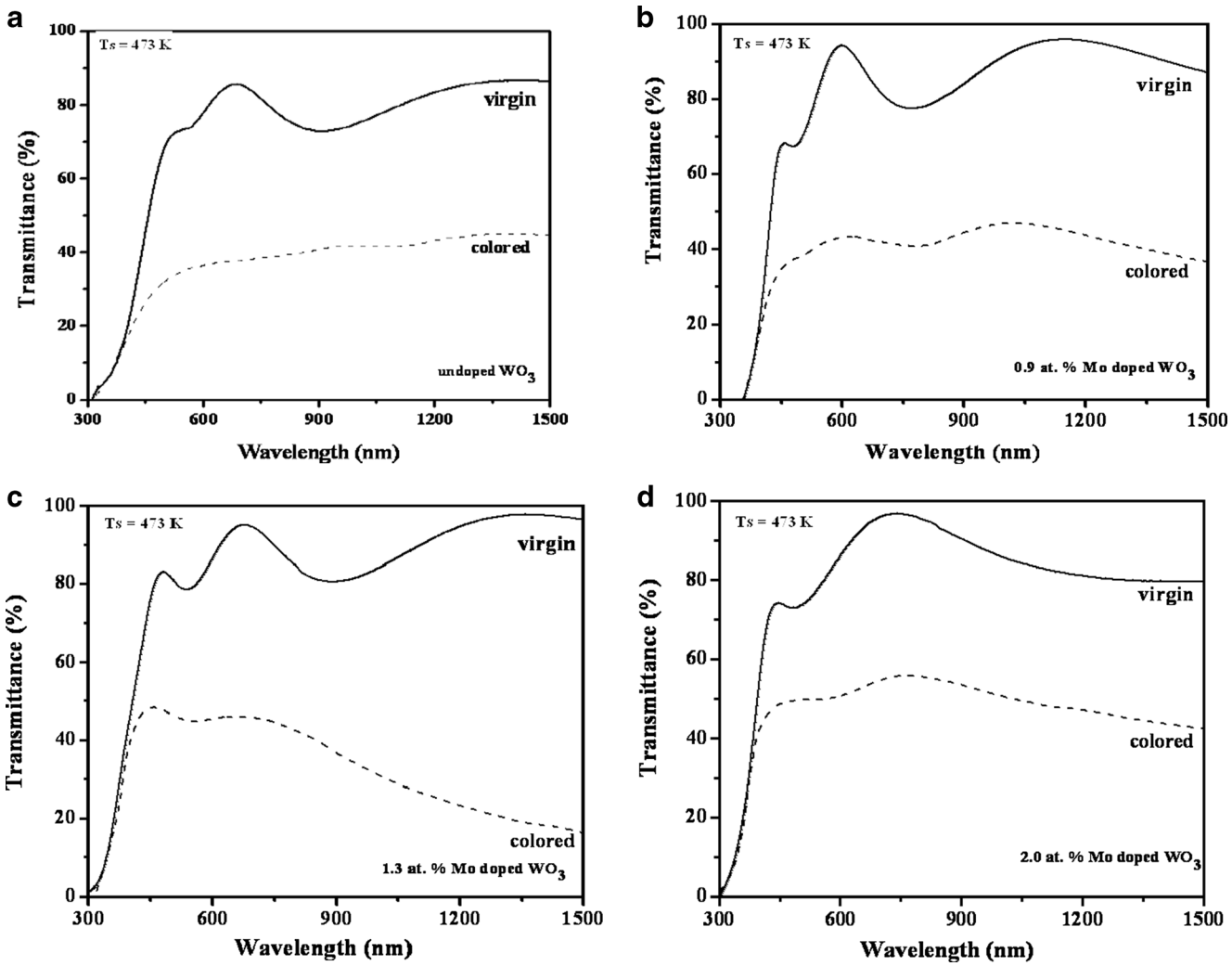

Fig. 10 Optical transmittance spectra of virgin and colored states of **a** pure WO_3 and **b** 0.9 at.%, **c** 1.3 at.% and **d** 2.0 at.% Mo-doped WO_3 films deposited on ITO-coated glass substrates formed at substrate temperature of 473 K

Electrochromic properties

Figure 10 shows the optical transmittance spectra of pure and Mo-doped WO_3 films deposited on ITO-coated glass substrates in virgin and colored conditions. The optical modulation is one of the important parameter to estimate the electrochromic quality of the electrode. The change in the optical modulation was estimated by $\Delta T = T_b - T_c$, where T_b and T_c are the transmittance for virgin and colored states at a wavelength of 550 nm. Figure 11 shows the variation of optical modulation with doping content of Mo in the WO_3 films. It is observed that the optical modulation increased from 40 % to 44.3 % with the increase of Mo content from 0 to 1.3 at.% and it decreased to 41.5 % at Mo dopant of 2.0 at.%. The coloration efficiency (η) is defined as the change in the optical density which changes intercalated per unit area of electrode. The coloration efficiency of the films was calculated by using the relation

$$\eta = (\Delta OD)/(Q/A) = [\log(T_b/T_c)/(Q/A)], \quad (9)$$

where ΔOD is the optical density, Q the charge inserted into the films and A the area of the films. Figure 11 shows the dependence of coloration efficiency on the Mo dopant content in the WO_3 films. It is observed that the coloration efficiency increased from 33.8 to 42.5 cm^2/C with the increase of Mo concentration from 0 to 1.3 at.%, respectively. The enhanced intercalation properties of Mo-doped WO_3 films was due to the rearrangement of atoms in the WO_3 crystal structure caused by the substitution of Mo ions at the W sites. Chen et al. [28] reported the coloration efficiency 25 cm^2/C in pure WO_3 films deposited by RF magnetron sputtering. Faughnan and Crandall [8] reported that the enhancement of electrochromic properties in mixed oxide films due to the inter-valance charge transfer between Mo^{5+} and W^{6+} sites. At further increase of Mo concentration to 2 at.%, the coloration efficiency decreased to 38 cm^2/C. This indicated that an appropriate doping concentration of molybdenum in WO_3 concentration play an important role to improve the electrochromic properties. Kondrachova et al. [12] reported that the coloration efficiency was increased from 29 to 34 cm^2/C with increase in Mo concentration. Hence, it is clearly indicated that the 1.3 at.% Mo-doped WO_3 films exhibit better electrochromic properties.

Conclusions

Thin films of Mo-doped WO_3 were deposited on ITO and glass substrates held at temperature of 473 K by RF magnetron sputtering technique. The deposited films were characterized for their chemical composition, crystalline structure, surface morphology, optical and electrochromic properties. The XRD studies on pure WO_3 films indicated that microcrystallites with orthorhombic structure were in the amorphous matrix. As the Mo dopant concentration increased the films undergo transformation from polycrystalline to amorphous structure. The crystallite size of 0.9 at.% Mo-doped WO_3 film was 24 nm and it was decreased with increase of dopant concentration. The scanning electron microscopy results showed different morphologies as the Mo doping concentration increased. The WO_3 films composed of grain-like structure which transformed to leaf-like structures with increase of doping of molybdenum dopant concentration from 0 to 2.0 at.%, respectively. The optical band gap and refractive index were increased with increase of Mo dopant concentration in WO_3 films. The electrochemical studied showed high anodic current density of 0.49 mA/cm^2 and diffusion coefficient of 8.5×10^{-11} cm^2/s in 1.3 at.% Mo-doped WO_3 films. The better electrochromic performance with high coloration efficiency of about 42.5 cm^2/C was obtained at 1.3 at.% doping of Mo in WO_3 films.

Acknowledgments One of the authors, V. Madhavi, is thankful to the University Grant Commission, India for the award of UGC - RFSMS Junior Research Fellowship to carry out the present work.

References

1. Granqvist CG (1995) Handbook of inorganic elecrochromic materials. Elsevier, Amsterdam
2. Cai GF, Zhou D, Xiong QQ, Zhang JH, Wang XL, Gu CD, Tu JP (2013) Sol Energy Mater Sol Cells 117:231
3. Noerochim L, Wang JZ, Wexler D, Chao Z, Liu HK (2013) J Power Sources 228:198
4. Qin Y, Fan G, Liu K, Hu M (2014) Sensors Actuators B 190:141
5. Hari Krishna K, Hussain OM, Julien CM (2010) Appl Phys A Mater Sci Process 99:921
6. Madhavi V, Kondaiah P, Subba Rayudu S, Hussain OM, Uthanna S (2013) Mater Express 5:135
7. Zheng H, Ou JZ, Strano MS, Kaner RB, Mitchell A, Kalantar-zadeh K (2011) Adv Funct Mater 21:2175
8. Faughnan BW, Crandall RS (1977) Appl Phys Lett 31:834
9. Bathe SR, Patil PS (2008) Solid State Ionics 179:314
10. Rougier A, Blyr A, Garcia J, Zhang Q, Impey SA (2002) Sol Energy Mater Sol Cells 71:343
11. Penin N, Rougier A, Laffont L, Poizot P, Tarascon JM (2006) Sol Energy Mater Sol Cells 90:422
12. Kondrachova L, Benjamin PH, Vijayaraghavan G, Williams RD, Stevenson KJ (2006) Langmuir 22:10490
13. Gesheva K, Cziraki A, Ivanova T, Szekeres A (2005) Thin Solid Films 492:322
14. Rueda de Leon JMO, Acosta DR, Pal U, Castaneda L (2011) Electrochim Acta 56:2599
15. Kalidindi NR, Manciu FS, Ramana CV (2011) ACS Appl Mater Interfaces 3:863
16. Kalidindi NR, Bharathi KK, Ramana CV (2011) Appl Phys Lett 97: 142107
17. Lethy KJ, Beena D, Mahadevan Pillai VP, Ganesan V (2008) J Appl Phys 104:033515
18. Lethy KJ, Beena D, Mahadevan Pillai VP, Ganesan V (2009) J Phys D Appl Phys 42:85407

19. Cullity BD (1978) Elements of X-ray diffraction, 2nd edn. Addition-Wesley, Reading, MA
20. Kovendhan M, Joseph DP, Kumar ES, Sendilkumar A, Manimuthu P, Sambasivam S, Venkateswaran C, Mohan R (2011) Appl Surf Sci 257:8127
21. Papadimitropoulos G, Vourdas N, Giannakopoulos K, Vasilopoulou M, Davazoglou D (2011) J Appl Phys 109:103527
22. Gullapalli SK, Vemuri RS, Ramana CV (2010) Appl Phys Lett 96: 171903
23. Gaury J, Kelder EM, Bychkov E, Biskos G (2013) Thin Solid Films 534:32
24. Swanepoel R (1983) J Phys E Sci Instrum 16:1214
25. Patil CE, Jadhav PR, Tarwal NL, Deshmukh HP, Karanjar MM, Patil PS (2011) Mater Chem Phys 126:711
26. Mahajan SS, Mujawar SH, Shinde PS, Inamder AI, Patil PS (2009) Sol Energy Mater Sol Cells 93:183
27. Nicholson RS, Shain I (1964) Anal Chem 36:706
28. Chen HS, Jan DJ, Chen CH, Huang KT (2013) Electrochem Acta 93:307